A Novel Xenograft Model Demonstrates Human Fibroblast Behavior During Skin Wound Repair and Fibrosis

Mimi R. Borrelli,[1,†] Abra H. Shen,[1,†] Michelle Griffin,[1,†] Shamik Mascharak,[1] Sandeep Adem,[1] Nestor M. Diaz Deleon,[1] Ledibabari Mildred Ngaage,[1] Michael T. Longaker,[1,2] Derrick C. Wan,[1] and Hermann Peter Lorenz[1,*]

[1]*Division of Plastic and Reconstructive Surgery, Department of Surgery, Stanford University School of Medicine, Stanford, California, USA.*
[2]*Department of Surgery, Institute for Stem Cell Biology and Regenerative Medicine, Stanford University School of Medicine, Stanford, California, USA.*
[†]*All these authors contributed equally to this work.*

Hermann Peter Lorenz, MD

Submitted for publication January 17, 2021. Accepted in revised form August 31, 2021.

*Correspondence: Division of Plastic and Reconstructive Surgery, Department of Surgery, Stanford University School of Medicine, Stanford, CA 94305-5148, USA
(e-mail: plorenz@stanford.edu).

Objective: Xenografts of human skin in immunodeficient mice provide a means of assessing human skin physiology and its response to wounding.
Approach: We describe a novel xenograft model using full-thickness human neonatal foreskin to examine human skin wound repair. Full-thickness 8 mm human neonatal foreskin biopsies were sutured into the dorsum of NOD scid gamma (NSG; NOD.Cg-Prkdc ^{scid}Il2rg^{tm1Wjl}/SzJ) pups as subcutaneous grafts. At postnatal day 21 the subcutaneous grafts were exposed to cutaneous grafts. Following maturation of 2 months, xenografts were then wounded with 5 mm linear incisions and monitored until postwound day (PWD) 14 to study skin repair and fibrosis. To explore whether our model can be used to test the efficacy of topical therapies, wounded xenografts were injected with anti-fibrotic fibroblast growth factor 2 (FGF2) for the first four consecutive PWDs. Xenografts were harvested for analysis by histology and fluorescence-activated cell sorting (FACS).
Results: Xenografts were successfully engrafted with evidence of mouse-human anastomoses and resembled native neonatal foreskin at the gross and microscopic level. Wounded xenografted skin scarred with human collagen and an expansion of CD26-positive human fibroblasts. Collagen scar was quantitated by neural network analysis, which revealed distinct clustering of collagen fiber networks from unwounded skin and wounded skin at PWD7 and PWD14. Collagen fiber networks within FGF2-treated wounds at PWD14 resembled those in untreated wounded xenografts at PWD7, suggesting that FGF2 treatment at time of wounding can reduce fibrosis.
Innovation and Conclusion: This novel xenograft model can be used to investigate acute fibrosis, fibroblast heterogeneity, and the efficacy of anti-fibrotic agents during wound repair in human skin.

Keywords: fibrosis, xenograft, fibroblast heterogeneity, scarring

DOI: 10.1089/wound.2020.1392

INTRODUCTION

WOUND HEALING CAN BE studied through a variety of assays, including *in vitro* and *in vivo* models.[1,2] Typically, *in vitro* assays are usually performed in the conventional two-dimensional (2D) cell monolayer format and assess cell migration, viability, and proliferation.[1,2] However, 2D assays are limited as they do not accurately mimic the complex cell-to-cell and cell–extracellular matrix interactions observed during wound healing.[1,2] Many acute mouse wound healing models have been developed, including incisional, excisional, and burn models.[1,2] However, wound healing and fibrosis of human skin are difficult to accurately recapitulate *in vivo* using current mouse and other animal models. There are numerous and significant anatomical and physiological differences between human and mouse skin[1,2]: mice have thinner epidermal, dermal, and subcutaneous layers; a distinct panniculus carnosus (limited in humans to the platysma in the neck and the scrotal dartos); absent sweat glands except on their paws; looser attachment of the dermis and epidermis; and a coat of hair that cycles synchronously, unlike the asynchronous growth of human hair.[1–4] Most importantly, mice heal skin wounds primarily by contraction, whereas human skin heals by re-epithelialization, limiting the ability of mice to form hypertrophic scars.[5,6] Pig skin is more similar to human skin, and porcine models have been reported to develop hypertrophic-like scars following deep wounds, but such models are expensive to maintain.[7,8] Consequently, current animal models cannot accurately recreate human skin pathologies,[9] and the majority of novel drugs proven efficacious in preclinical studies in mice have been unsuccessful upon translation to humans.[10,11] Alternative *ex vivo* models, where whole skin biopsies are cultured, have been utilized to examine tissue fibrosis.[12] While *ex vivo* models offer a system that closely resembles human skin, they are limited to analyzing the immediate and short time evaluation of cells compared to *in vivo* models.[12]

CLINICAL PROBLEM ADDRESSED

Xenografts of human skin on immunodeficient mice provide a more translatable means of assessing human skin physiology during homeostasis, following wounding, and in response to different antifibrotic treatments. Xenograft models are still limited by their inability to evaluate the inflammatory response following wounding but offer the ability to assess the response of human skin to wounding.[13,14] Although various human skin xenograft models and techniques have been described, current methods are limited by poor engraftment of full-thickness human skin and variability of skin samples across age, gender, body site, and sun exposure.[13,14] The NOD-*scid* mouse strain with the interleukin-2 receptor gamma chain (*IL2rg*)-targeted mutation (NOD.Cg-*Prkdc*^{scid} *IL2rg*^{tm1Wjl}/Sz, NOD scid gamma, or NSG) has minimal host-graft rejection, which allows xenografted human tissue and cells to survive for extended periods of time.[13,14] The NSG strain has been successfully used to create xenograft models for study of hematopoietic and immune cells.[15–17] We describe a novel NSG xenograft model to study human skin *in vivo* and its response to different fibrosing conditions. Furthermore, we evaluated fibroblast growth factor 2 (FGF2), one of the members of the mammalian FGF family, as it is a cytokine associated with antifibrotic activity in animal and *in vitro* models.[18] FGF2 has been shown to inhibit and antagonize differentiation of myofibroblasts, suppressing profibrotic gene expression, alleviating fibrosis.[19,20] We demonstrate that the xenograft model may be useful to examine the effect of potential and mechanism of antifibrotic agents.

MATERIALS AND METHODS

Animals

NSG (NOD.Cg-*Prkdc*^{scid} *Il2rg*^{tm1Wjl}/SzJ) immunodeficient mice ($n = 30$) purchased from the Jackson laboratories (No. 005557; JAX) were used for all xenografting experiments. Mice were operated on at postnatal days 5–7 (P5–7). Animals were maintained at Stanford University animal core facility in accordance with Stanford and National Institutes of Health guidelines under an approved APLAC protocol (No. 32993).

Establishment of human neonatal foreskin xenograft

Human neonatal foreskin ($n = 10$) was obtained from routine neonatal circumcisions performed at Stanford Hospital under an approved Institutional Review Board (IRB; No. 35711). Fresh, full-thickness circular 8 mm biopsies of neonatal foreskin tissue were transplanted beneath the skin panniculus carnosus on the dorsum of NSG pups aged between P5–7 using a protocol adapted from our previous work (Fig. 1a).[21] Mouse dorsal skin was first cleaned with ethanol and betadine. The subpanniculus/subcutaneous space was then entered by creating a 6 mm linear incision made using a scalpel in the rostral to caudal direction and using blunt dissection with sterile scissors. The

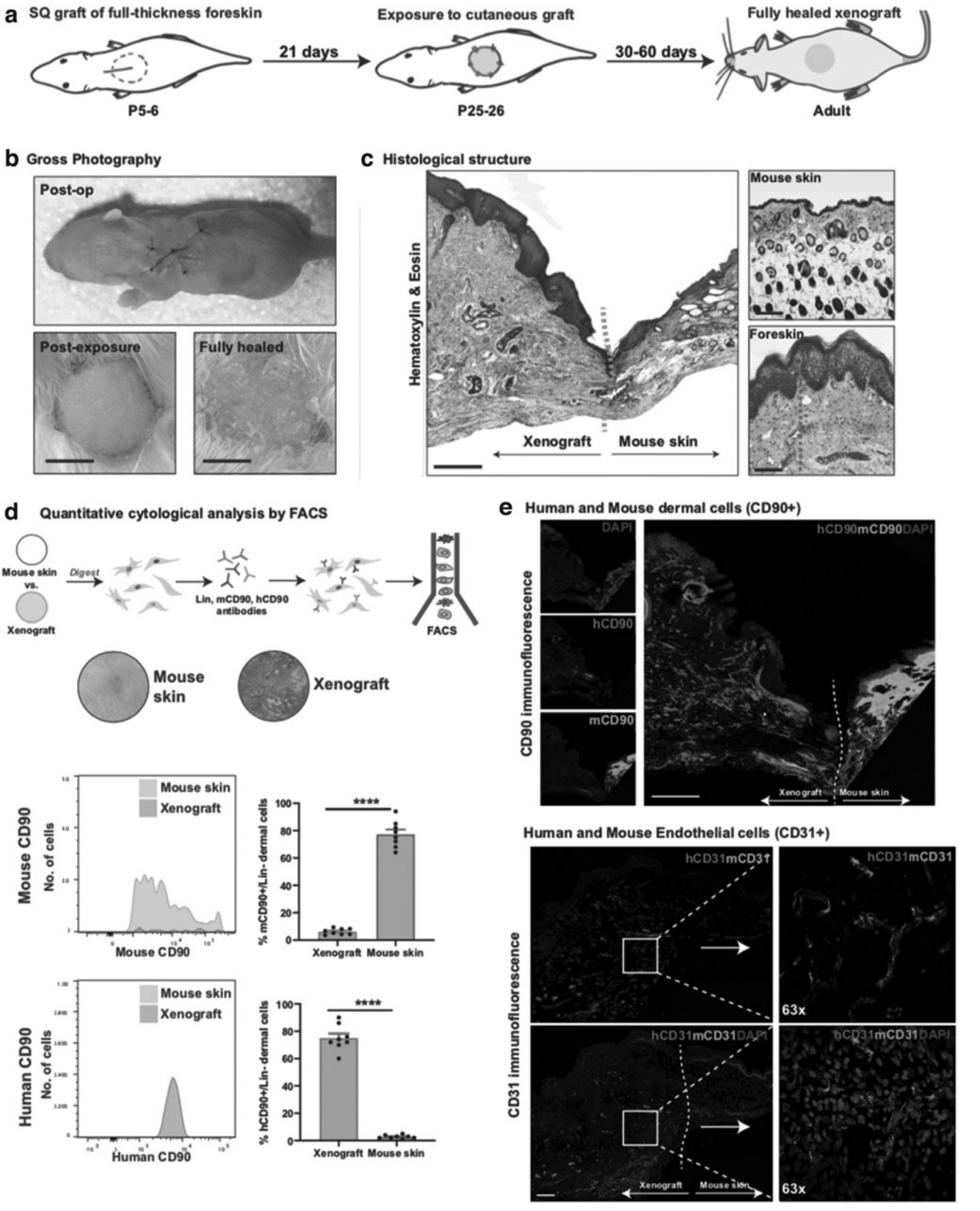

Figure 1. The human xenografted skin survives and exhibits a micro- and macroscopic resemblance to unwounded human neonatal foreskin: **(a)** graphical representation of the steps involved in the grafting of the human foreskin skin. **(b)** Representative gross image of a healed xenograft. Scale bar: 500 μm. **(c)** H&E-stained xenografted human skin. The *orange dotted line* shows the border separating mouse skin and grafted human neonatal foreskin, and the *green dotted lines* represent dermis thickness. Scale bar: 200 μm. **(d)** Xenografted skin and adjacent normal mouse skin were analyzed by FACS for presence of mouse- and human-specific fibroblasts (Lin-CD90$^+$ live dermal cells). **(e)** *Top:* Immunofluorescence staining for mouse- (*green*) and human-specific (*red*) CD90$^+$ cells. Scale bar: 200 μm. The *white dotted line* shows the border separating mouse skin and grafted human neonatal foreskin. *Bottom*: Immunofluorescence staining for mouse- (*green*) and human-specific (*red*) endothelial cells (CD31/PECAM), with *white dotted line* demonstrating overlap and likely anastomoses between mouse and human vessels. Scale bar: 50 μm. ****$p < 0.0001$. FACS, fluorescence-activated cell sorting; H&E, hematoxylin and eosin.

foreskin biopsies were placed into the subcutaneous pocket epidermis side up and anchored to the overlying skin using four simple interrupted stitches (Nylon 6′0, Ethilon). The mouse dorsal skin pocket was then closed over the xenograft with a single mattress suture. Cyanoacrylate (Loctite) was used to secure the sutures in place. At P21, the grafts were exposed to become cutaneous grafts by removing the mouse skin overlying the xenograft, freeing the xenograft from the capsule of fibrotic mouse tissue that inevitably forms over the xenografted skin, and securing the newly exposed human skin xenograft to the surrounding mouse skin using four interrupted sutures (Nylon 6′0, Ethilon). Xenografts were covered with occlusive dressings (3M Tegaderm), which were changed every other day for 14 days. The xenografts were then observed for 2 months as they matured.

Xenograft wounding and fibrosis

To model acute fibrosis, xenografts that had matured to postoperative day (POD) 60 were wounded with 5 mm long linear incisions created using a No. 11 scalpel. Wounds penetrated a maximum depth of 3 mm into the xenograft skin. Care was taken to ensure that the xenograft wounds were not made full thickness through the graft and into the underlying mouse capsular tissue. The wounds were followed by gross inspection over the subsequent 14 postwound days (PWDs). To model the use of xenografted human skin as a platform for testing the efficacy of topical agents, xenograft wounds were injected with human FGF2 (No. PHG6015; Thermo Fisher Scientific). Peri-wound intradermal injections of FGF2 were made on PWDs 1, 2, 3, and 4 (100 μL phosphate buffered saline [PBS] containing 1 μg of FGF2), following methods described previously.[22]

Histology

Mice were euthanized on PWD14, and skin was harvested for histological analysis. Specimens were fixed in 4% paraformaldehyde (PFA, No. 15710; Electron Microscopy Sciences) at 4°C for 18 h, dehydrated in dilutions of ethanol, and embedded in paraffin for sectioning at 8 μm. Sections were stained with hematoxylin and eosin (H&E, No. ab245880; Abcam) for assessment of dermal thickness, with Masson's Trichrome (No. ab150686; Abcam) for visualization of dermal collagen and with Picrosirius Red (No. ab150681; Abcam) for assessment of collagen fiber networks. Standard staining protocols were followed. Slides were imaged using the Leica DM5000 B light microscope (Leica Microsystems, Buffalo Grove, IL) at 10× and 20×. Polarized light and the 40× objective were used to image Picrosirius-stained slides. Imaris software (imaris.oxinst.com) was used to visualize fluorescent images, and images were analyzed for positive pixel staining using ImageJ (imagej.nih.gov).

Immunofluorescence

Paraffin-sectioned slides were prepared for immunofluorescence images. Sections were first deparaffinized with xylene, gradually rehydrated with decreasing concentrations of ethanol, and then treated with Trypsin Antigen-Retrieval Solution (No. ab970; Abcam). Sections were first blocked with 1×Power Block (No. HK083-50K; BioGenex) and then incubated for 1 h at 37°C with primary antibodies at a 1:100 dilution in 0.1×Power Block. Slides were then washed in PBS (No. 10010023; Gibco) and then incubated with secondary antibodies at a 1:100 dilution in 0.1×Power Block. Finally, slides were washed in PBS and mounted with a coverslip using DAPI Fluoromount-G (No. 0100-20; SouthernBiotech). Fluorescent z-stack (8 μm depth) tiled images were taken using the LSM 880 inverted confocal microscope (Airyscan, GaAsP detector, 880; Beckman), using standard field size for each tile (1,024×1,024).

The following primary antibodies were used: Anti-human-CD90 (No. ab133350; Abcam), anti-mouse-CD90 (No. ab3105; Abcam), anti-human-CD31 (No. ab32457; Abcam), anti-mouse-CD31 (No. ab7388; Abcam), anti-human- collagen type I alpha I (No. ab82504; Abcam), anti-mouse-collagen type I alpha I (No. ab21286; Abcam), and anti-human-CD26 ("DDP4," No. ab119346; Abcam).

The following secondary Alexa Flour (AF)-conjugated antibodies were used: AF488 (No. A11034 [Thermo Fisher Scientific], No. ab150173 [Abcam], and No. ab150157 [Abcam]) and AF647 (No. A31573 [Thermo Fisher Scientific], No. ab150075 [Abcam], and No. ab150159 [Abcam]).

Fluorescence-activated cell sorting

Fibroblasts were isolated from xenografts and mouse skin for analysis by fluorescence-activated cell sorting (FACS) at PWD14. Skin samples were first dissected using sterile scissors, washed in PBS (No. 10010023; Gibco), cut into 2 mm thick strips using scissors, and submerged in Dispase (25 U/mL, No. CB40235; Corning, Fisher Scientific) in Dulbecco's modified Eagle's medium (DMEM) GlutaMAX (No. 10566-016; Thermo Fisher Scientific) for 18 h at 4°C to facilitate enzymatic epidermal–dermal separation. After incubation, the epidermis was removed with sterile forceps and discarded. Dermal skin was then mechanically digested using sterile curved scissors until consistency was reached and incubated with Collagenase (Type IV,

1,500 U/mL, No. 17104019; Fisher Scientific) in Hanks Buffered Saline Solution (HBSS, No. 14025076; Thermo Fisher Scientific) under constant agitation (150 rpm) at 37°C for 30 min. The enzyme was then quenched with FACS buffer (2% fetal bovine serum, 1% pluronics [No. 24040032; Thermo Fisher Scientific], 1% Penicillin-streptomycin) in a 1:1 ratio, resuspended in 500 μL of FACS buffer, carefully pipetted onto 1 mL of Histopaque (1.119 g/mL, No. 11191; Sigma-Aldrich), and centrifuged (400 *g*, 15 min, room temperature [RT], without deceleration) for further purification by density gradient separation. The buffy coat (containing dermal cells) was retrieved by pipette, washed in PBS, pelleted, and resuspended in 100 μL for staining with fluorophore-conjugated antibodies against human and mouse lineage cells: human(h)CD45-eFluor450 (No. 304029-BL; BioLegend) and mouse(m)CD45-eFluor450 (No. 48–0451-82; BioLegend) to label hematopoietic cells; hCD235a-eFluor450 (No. 306612-BL; BioLegend) and mTER-119-eFluor450 (No. 48-5921-80; eBioscience) to label erythrocytes; hCD31eFluor450 (No. 13-0319-82; Thermo Fisher Scientific) and mCD31-eFluor450 (No. 48–0311; eBioscience) to label endothelial cells; mCD202b-Biotin (Tie-2, No. 13–5987-81; eBioscience) to label pericytes; and mEpCAM (epithelial cell adhesion molecule, CD326)-eFluor450 (No. 48-5791-80; eBioscience) and mCD324-eFluor450 (eCadherin, No. 13-3249-80; eBioscience) to label epithelial cells. In addition, human and mouse antibodies to CD90 ("Thy1") were used to positively gate for human and mouse fibroblasts (as $CD90^{+}$lin-LIVE dermal cells); hCD90-AF700 (No. 56-0909-42; Thermo Fisher Scientific) and mCD90-APC (No. 17-0900-82; eBioscience). Primary antibodies were used in a 1:100 dilution for 30 min at 4°C in the dark. Secondary antibody staining was performed with the streptavidin-eFluor-450 conjugated antibody (No. 48-4317; eBioscience) for 20 min at 4°C in the dark. Live-dead staining was achieved with DAPI (1:10,000 dilution, No. 62248; Thermo Fisher). FACS was performed on the FACS Aria II (BD Biosciences, The Beckman Center). Gating schemes were established with fluorescence-minus-one (FMO: staining with all fluorophores except one) controls.

Computational analysis of collagen fiber networks

To model collagen fiber networks, images of Picrosirius Red-stained slides were color deconvoluted, converted to gray scale, binarized, and skeletonized using a novel algorithm run in MATLAB (R2018b; MathWorks, Natick, MA).[23] Thirteen parameters of red collagen fibers were extracted from skeletonized images (brightness, number, length, width, persistence, angle, branch points, Euler number, extent, perimeter, solidity, eccentricity, equivalent diameter). Parameters underwent dimensionality reduction to generate 2D t-Distributed Stochastic Neighbor Embedding (TSNE) plots to visualize collagen fiber network patterns in four different types of xenograft; (1) unwounded, (2) PWD7 (mid-healing), (3) PWD14 (fully healed/scarred), and (4) FGF2-treated wounds harvested at PWD14. A total of 100 images from 5 wounds per xenograft condition were used for analysis. Geometric shapes were drawn to approximate the distribution of each cluster.

Statistical analyses

Statistical analyses were performed on GraphPad Prism (www.graphpad.com). Data are presented as mean and standard error of the mean. Means were compared using the unpaired *t*-test (two-tailed) and the analysis of variance with Bonferroni test for *post hoc* analysis. A *p*-value of $*<0.05$ was considered significant. Electronic laboratory notebook was not used.

RESULTS

Human xenografted skin has the macro- and microscopic appearance of unwounded human skin

Gross photography assessment of healed xenografts in adult NSG mice revealed human-appearing skin, distinct from the surrounding mouse skin (Fig. 1b). Histological assessment using H&E revealed the human xenografted skin to have thicker epidermal and dermal layers than surrounding mouse skin, as well as an absence of hair follicles, resembling ungrafted neonatal foreskin (Fig. 1c).

Human skin xenografts were mostly composed of human fibroblasts

FACS analysis for cytological quantification revealed that 77.4% of the cells isolated from the human xenografted skin dermis were human CD90 positive (Fig. 1d). Immunostaining for spatial localization of mouse and human fibroblasts confirmed that the human xenografted skin was comprised primarily of human CD90-positive dermal cells (fibroblasts), and the mouse dermis was comprised primarily of mouse CD90-positive cells (Fig. 1e).

Human xenografts become vascularized by anastomoses between mouse and human vessels

The vasculature of xenografted skin was evaluated for host species of origin by staining for mouse- and human-specific CD31. Analysis revealed blood

vessels in the human skin xenograft to contain both mouse and human endothelial cells with evidence of anastomoses (Fig. 1e).

Human xenografted skin can be used to model acute fibrosis and scarring

Wounded xenografted skin had completely healed by PWD14 with a visible scar on gross inspection (Fig. 2a). Tissue sections from PWD14 wounds stained with H&E and Masson's Trichrome revealed regions of low cellularity and high collagen fiber density in the papillary dermis, corresponding to scars at the incised area (Fig. 2b, c). Immunostaining for mouse- and human-specific collagen type I confirmed that the area of fibrosis was primarily composed of human-specific collagen type I (Fig. 2d). Quantitative analysis of the collagen fiber networks in unwounded and PWD14 xenografted from images of Picrosirius Red-stained slides revealed little overlap in the collagen fiber networks between unwounded xenografts and wounded xenografts at PWD14 (Fig. 2e), consistent with induction of acute fibrosis upon wounding.

Human xenografted skin can be used to explore human fibroblast heterogeneity

FACS analysis was used to quantitatively compare numbers of profibrotic CD26-positive fibroblasts in unwounded and unwounded xenografted skin. FACS analysis confirmed that CD26-positive fibroblasts significantly increased in response to wounding (unwounded [UW] vs. PWD14, $^{****}p < 0.0001$) (Supplementary Fig. S1a). CD26 marks profibrotic fibroblast populations[24]; thus, these data further corroborate their induction upon wounding and acute fibrosis and highlight how this xenograft model can be used to investigate human fibroblast heterogeneity. Immunostaining was used for spatial localization and confirmed that CD26-positive cells populated the papillary dermis (Supplementary Fig. S1b), consistent with known data on CD26-positive fibroblasts.[25,26]

The human skin xenograft model is a platform for exploring antifibrotic agents

FGF2-treated wounds had healed by PWD14 and appeared soft and vascular with no visible scar on gross inspection (Fig. 3a) nor on histological analysis, with histologic evidence of epidermal hyperplasia (Fig. 3b, c). As FGF2 is known to be a potent proangiogenic growth factor,[27] the FGF2-treated and untreated xenografts were immunostained for mouse- and human-specific CD31. Results indicated significantly increased vascularity in the FGF2-treated wounds compared to unwounded skin ($^{***}p < 0.001$) and that the vessels were primarily composed of human endothelial cells (Fig. 3d, e). Interestingly, we observed that FGF2-treated wounds reduced the density of collagen staining in wounded xenografts, compared to wounded but untreated xenografts, as shown by Masson's Trichrome (Fig. 3c). We therefore subjected the images of Picrosirius Red-stained slides to collagen fiber network analysis. Results indicated that the collagen fiber networks in PWD14 wounds treated with FGF2 strongly overlapped with the collagen fibers comprising earlier wound time points (at PWD7) (Fig. 3d), suggesting that FGF2 treatment reduced fibrosis at PWD14.

DISCUSSION

We describe a novel model and pipeline for exploring human fibroblast heterogeneity and human fibroblast behavior during skin wound repair and fibrosis. Our technique of grafting full-thickness human neonatal foreskin initially as subcutaneous grafts with subsequent exposure to the cutaneous position produces viable human neonatal skin *in vivo* that resembles ungrafted neonatal foreskin at macroscopic and microscopic levels. We demonstrate, using histology and FACS, that the xenografted skin dermis is composed almost entirely of human CD90-positive fibroblasts, demonstrating successful engraftment (Figs. 1 and 2 and Supplementary Fig. S2). The confirmation of vascular anastomoses between the human and mouse vasculature, with the majority of blood vessels within the xenografts comprised of human endothelial cells, highlights the potential long-term survival of the xenograft.

To demonstrate how our xenograft model can be used to study human skin wound healing, we cre-

Figure 2. The xenograft model can be used to model acute fibrosis and fibroblast heterogeneity. **(a)** Graphical representation wounding of the xenograft. **(b)** Gross images of a representative wounded xenograft at PWDs 0 through 14. **(c)** Representative wounded xenograft at PWD14 stained with H&E. *Narrow black* and *white dotted lines* depict the scar and *thicker lines* at the xenograft-mouse skin junction. Scale bar: 100 μm. **(d)** Immunofluorescence staining for mouse- (*green*) and human-specific (*red*) collagen type I alpha I. *Narrow white dotted line* depicts the scar, and *thicker white line* is the xenograft-mouse skin junction. Scale bar: 100 μm. **(e)** Picrosirius Red-stained images of unwounded and wounded xenografts at PWD14 were subjected to computational algorithm which extracted 13 parameters of collagen fiber networks. The networks underwent dimensionality reduction to generate 2D TSNE plots of fibers in unwounded skin (*yellow dots/outline*) and PWD14 healed (scarred, *red dots/outline*). Distinct collagen patterns are demonstrated between unwounded skin and wounded skin at PWD14. 2D, two-dimensional; PWD, postwound day; TSNE, t-Distributed Stochastic Neighbor Embedding.

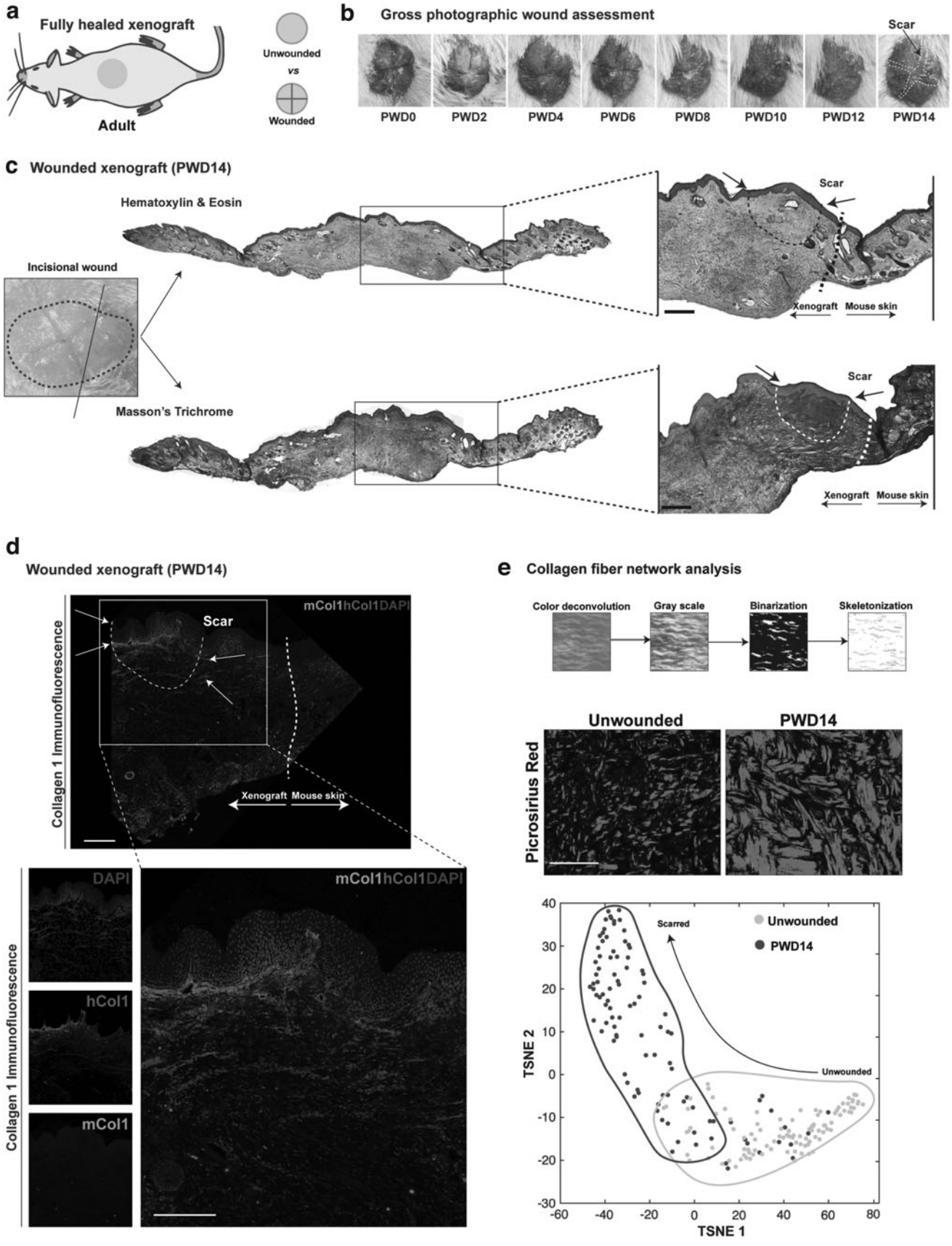
a
Fully healed xenograft
Adult
Unwounded
vs
Wounded
b
Gross photographic wound assessment
Scar
PWD0
PWD2
PWD4
PWD6
PWD8
PWD10
PWD12
PWD14
c
Wounded xenograft (PWD14)
Hematoxylin & Eosin
Incisional wound
Masson's Trichrome
Scar
Xenograft
Mouse skin
d
Wounded xenograft (PWD14)
Collagen 1 Immunofluorescence
mCol1hCol1DAPI
Scar
Xenograft
Mouse skin
DAPI
hCol1
mCol1
e
Collagen fiber network analysis
Color deconvolution
Gray scale
Binarization
Skeletonization
Unwounded
PWD14
Picrosirius Red
Scarred
Unwounded
PWD14
TSNE 1
TSNE 2

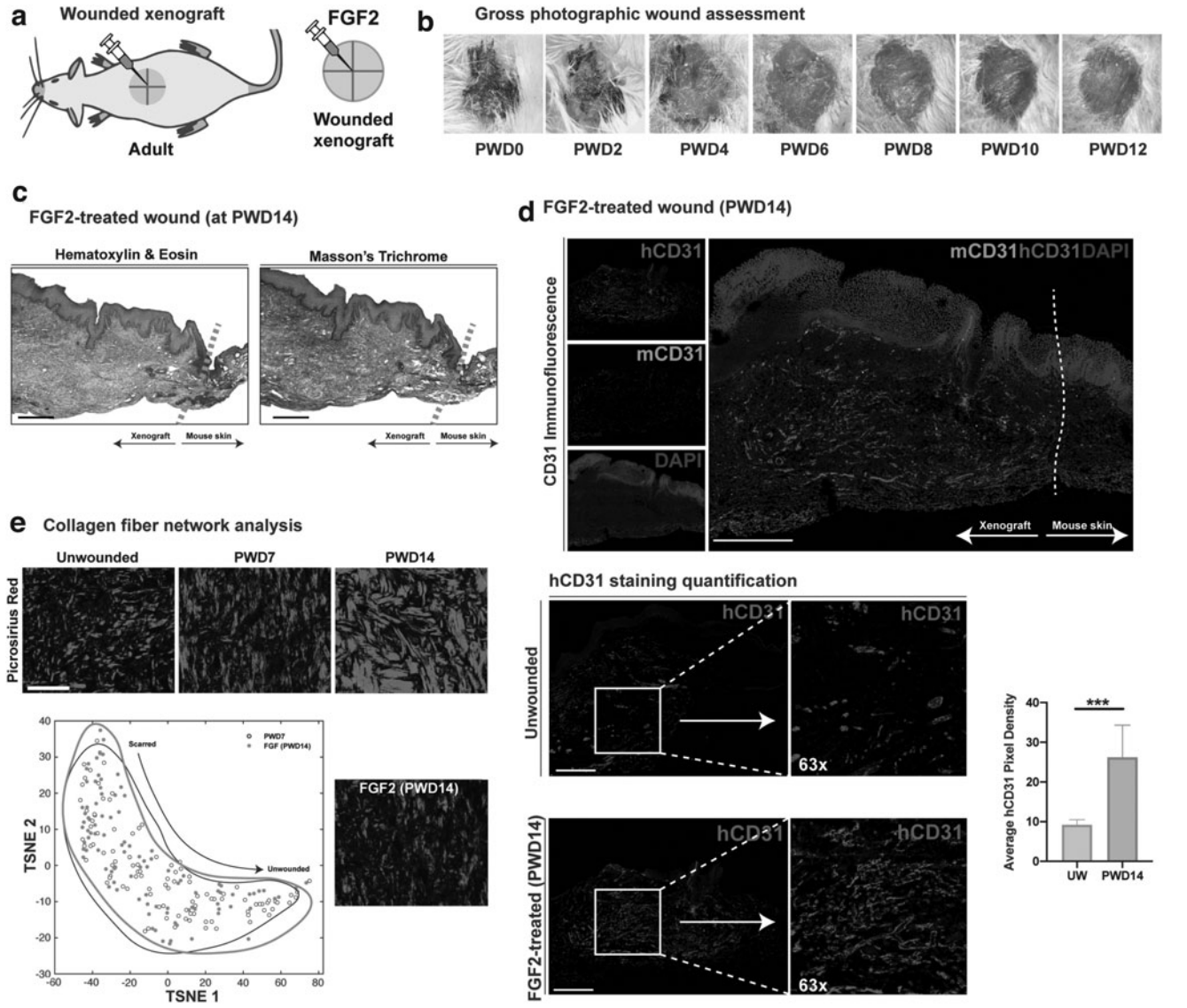

Figure 3. The xenograft model is a platform for exploring the efficacy of topical agents. **(a)** Graphical representation of the wounded and unwounded xenograft with FGF treatment. **(b)** Representative gross images of a FGF2-treated wound at PWDs 0 through 12. **(c)** Representative FGF2-treated wounded xenograft at PWD14 stained with H&E and Masson's Trichrome. Scale bar: 200 μm. **(d)** Immunofluorescence staining for mouse- (*green*) and human-specific (*red*) endothelial cells (CD31/PECAM). Scale bar: 200 μm. Quantitative comparison of mean pixels positive for hCD31 in unwounded and FGF2-treated wounds at PWD14. ***$p < 0.001$. **(e)** 2D TSNE plots of collagen fiber networks in PWD7 (*gray*) and FGF2-treated wounds at PWD14 (*black outline*), showing overlap with no distinct difference. FGF2, fibroblast growth factor 2.

ated linear wounds in the xenografted skin. At PWD14 the xenografted skin exhibited visible scars which were histologically composed of human collagen fibers. Quantitative analysis of collagen fiber networks revealed distinct patterns in the collagen fiber networks between unwounded xenografts and wounded xenografts at PWD14, consistent with the fibrotic nature of scarred skin. Wounds in our model were made in the superficial papillary dermis. By keeping the wound depth within the dermis of the xenograft, the mouse capsular tissue under the xenograft was not violated. This enables the wounds to heal with collagen produced by human fibroblasts, rather than mouse fibroblasts from the capsule. Although the degree of fibrosis and scarring was limited (*e.g.*, compared to an excisional wounding model), our collagen network analysis demonstrated nonoverlapping patterns between fibers from unwounded and wounded xenografts at PWD14. Specifically, the fibrosis patterns in wounded xenografts were distinct from those in unwounded xenografts.

We treated wounded xenograft skin with FGF2 to highlight the potential of our model as a platform

for testing the therapeutic efficacy of skin wound repair agents. FGF2 was chosen as it is a potent proangiogenic growth factor[27] with reported antifibrotic qualities.[28–31] As expected, we found that FGF2 treatment increased the density of blood vessels within the wounded xenografts. Interestingly, the FGF2-treated wounds healed with minimal scars on gross inspection and, histologically, had collagen fiber network patterns that overlapped with the network patterns observed at PWD7 in untreated wounds. This suggests that FGF2 had an antifibrotic effect. Future work can investigate longer time points postwounding to explore whether these effects are long lasting. Furthermore, further work will seek to investigate and characterize the presence or absence of antifibrotic effects of other predicted pharmacologic antifibrotic compounds. Finally, through immunostaining and FACS analysis, we show that the human xenografted papillary dermis is rich in CD26-positive fibroblasts and that this profibrotic fibroblast subpopulation within the graft selectively expands during wound repair. To our knowledge, this is the first study to provide data supporting human fibroblast heterogeneity during human wound repair. Our data are consistent with previous literature identifying CD26 as a marker of papillary dermal fibroblasts[25,26] and as a marker of fibroblasts with increased fibrotic potential in both mice and humans.[24,32] Together, these results indicate that our human xenograft skin model can be used to explore human skin fibrosis as it pertains to different human fibroblast subpopulations. Our model system has tighter control of experimental variables which may save both time and expense compared to human trials.

In this article we describe a human xenograft model which is significantly improved over our basic technique described in 1992.[21] In the current model, we uniquely combine both subcutaneous and cutaneous grafting techniques to further optimize our previous methodologies. The initial subcutaneous pocket facilitates engraftment and vascularization, while the cutaneous position exposes grafts to the air allowing for keratinization and a more human skin-like appearance due to this more physiological position. We used pups aged P5–7 to exploit the thin, regenerative vascular nature of juvenile recipient host tissue which likely enhances graft vascularization and survival. The use of neonatal foreskin allows for age- and sex-matched xenografts that have minimal photodamage, which helps ensure consistency between grafts for exploring the response of different treatment conditions.[33,34] The heterogeneity between different donors can also more accurately mimic the natural variation in human patients.[1] Finally, neonatal foreskin samples are thin and allow for the full dermis (papillary and reticular) to be transplanted. Other animal models using human neonatal skin grafts have been described. Petratos *et al.*, have described a xenograft model where human foreskin grafts are placed subcutaneously in nude rats with 100% viability.[35] However, graft viability was only confirmed 10 days post transplantation with no long-term follow-up or utilization of the model for investigating skin wound repair.[35]

Our xenograft model has limitations. The recipient NSG mice are immunosuppressed to minimize graft rejection.[36–38] This impairs the ability of our experimental model to completely study the human immune system during wound repair and interactions between the human immune and skin cells during fibrosis. Although the xenograft model is limited by its ability to fully assess the inflammatory response, which is an important determinant of wound healing, it allows human skin to be studied in terms of the microenvironment, cell–cell interactions, vasculature formation, and paracrine and autocrine signaling.[13,14] The presented xenograft model allows for extensive assessment of human skin wounds, which is important for clinical translation.[13,14] Future work could consider using bone marrow transplants of human immune cells to study this aspect of wound healing. Another limitation of the xenograft model is that the foreskin lacks hair, and consequently, *in vivo* human hair cycling cannot be modeled. Our xenograft model is, however, rich in other skin appendages, such as sebaceous and apocrine glands. This may be useful for studying their physiological niche, or exploring appendage transplantation, as well as a useful platform to study pharmaceutical treatments that target skin appendages, such as hyperhidrosis. In summary, this human skin xenograft mouse model better recapitulates the human wound healing process and is a significant advancement in our exploration of fibrosis and functional human fibroblast heterogeneity throughout wounding.

INNOVATION

This novel xenograft model of human neonatal foreskin is a platform for exploring the response of the human dermis to wounding and the potential of

antifibrotic agents. This *in vivo* platform may help to highlight potential cellular and molecular targets to treat skin scarring and improve wound healing, which may have significant implications for the field of plastic and reconstructive surgery.

KEY FINDINGS

- Scarring and fibrosis of human skin are difficult to mimic *in vivo* using animal models.
- We have produced a reproducible and novel xenograft model of human neonatal foreskin to explore Wound healing and fibrosis.
- The xenograft foreskin model can be used to study skin scarring and the role of antifibrotic agents.

AUTHORS' CONTRIBUTIONS

M.R.B., A.H.S., and M.G. performed the experiments, analyzed data, and wrote the final article. S.M. performed experiments and approved the final article. S.A., N.M.D.D., and L.M.N. performed experiments. M.T.L., D.C.W., and H.P.L. oversaw the experimental design and data analysis. All authors approved the final article.

ACKNOWLEDGMENTS AND FUNDING SOURCES

This work was supported by grants from the Oak Foundation and the Hagey Laboratory for Pediatric Regenerative Medicine. M.R.B. was supported by the Plastic Surgery Research Foundation (PSRF). M.G. was supported by the Fulbright Scholar Program. A.H.S. was supported by funding from the Sarnoff Cardiovascular Research Foundation. N.M.D.D. was supported by the California Institute for Regenerative Medicine (CIRM). M.T.L. was supported by the NIH grant R01 GM116892, Gunn/Olivier Research Fund, Stinehart-Reed Fund, and the NIH grant U01 HL099776. D.C.W. was supported by NIH DE027346. H.P.L. was supported by the NIH grant R01 GM116892.

AUTHOR DISCLOSURE AND GHOSTWRITING

No competing financial interests exist. The content of this article was expressly written by the authors listed. No ghostwriters were used to write this article.

ABOUT THE AUTHORS

Mimi R. Borrelli, MBBS, MSc, Abra H. Shen, SB, and **Michelle Griffin, MBBS, PhD,** are plastic surgery research fellows in Dr Longaker, Dr Wan, and Dr Lorenz's laboratories at Stanford University. **Shamik Mascharak, PhD,** is a student in Dr. Longaker's laboratory. **Sandeep Adem, MS, Nestor M. Diaz Deleon,** and **Ledibabari Mildred Ngaage, MA, Cantab, MB, BChir,** are research assistants in Dr Longaker, Dr Wan, and Dr Lorenz's laboratories at Stanford University. **Michael T. Longaker, MD, MBA,** is the Deane P and Louise Mitchel Professor at Stanford School of Medicine. **Derrick C. Wan, MD and H. Peter Lorenz, MD,** are Professors of Plastic and Reconstructive Surgery at Stanford University.

SUPPLEMENTARY MATERIAL

Supplementary Figure S1
Supplementary Figure S2

REFERENCES

1. Salgado G, Ng YZ, Koh LF, Goh CS, Common JE. Human reconstructed skin xenografts on mice to model skin physiology. Differentiation 2017;98: 14–24.
2. Gerber PA, Buhren BA, Schrumpf H, Homey B, Zlotnik A, Hevezi P. The top skin-associated genes: a comparative analysis of human and mouse skin transcriptomes. Biol Chem 2014;395: 577–591.
3. van der Veen C, Handjiski B, Paus R, et al. A comprehensive guide for the recognition and classification of distinct stages of hair follicle morphogenesis. J Invest Dermatol 1999;113:523–532.
4. Khavari PA. Modelling cancer in human skin tissue. Nat Rev Cancer 2006;6:270.
5. Wong VW, Sorkin M, Glotzbach JP, Longaker MT, Gurtner GC. Surgical approaches to create murine models of human wound healing. J Biomed Biotechnol 2010;2011:969618.
6. Ibrahim MM, Bond J, Bergeron A, et al. A novel immune competent murine hypertrophic scar contracture model: a tool to elucidate disease mechanism and develop new therapies. Wound Repair Regen 2014;22:755–764.
7. Zhu KQ, Engrav LH, Gibran NS, et al. The female, red Duroc pig as an animal model of hypertrophic scarring and the potential role of the cones of skin. Burns 2003;29:649–664.
8. Wang J, Ding J, Jiao H, et al. Human hypertrophic scar-like nude mouse model: characterization of the molecular and cellular biology of the scar process. Wound Repair Regen 2011; 19:274–285.
9. Elsea SH, Lucas RE. The mousetrap: what we can learn when the mouse model does not mimic the human disease. ILAR J 2002;43:66–79.
10. Hackam DG, Redelmeier DA. Translation of research evidence from animals to humans. JAMA 2006;296:1727–1732.

11. DiMasi JA, Grabowski HG, Hansen RW. Innovation in the pharmaceutical industry: new estimates of R&D costs. J Health Econ 2016;47: 20–33.

12. Ud-Din S, Bayat A. Non-animal models of wound healing in cutaneous repair: in silico, in vitro, ex vivo, and in vivo models of wounds and scars in human skin. Wound Repair Regen 2017;25:164–176.

13. Reed ND, Manning DD. Long-term maintenance of normal human skin on congenitally athymic (nude) mice. Proc Soc Exp Biol Med 1973;143:350–353.

14. Rygaard J. Skin grafts in nude mice. APMIS 1974; 82:80–92.

15. Ishikawa F, Yasukawa M, Lyons B, et al. Development of functional human blood and immune systems in NOD/SCID/IL2 receptor γ chainnull mice. Blood 2005;106:1565–1573.

16. Ito M, Hiramatsu H, Kobayashi K, et al. NOD/SCID/γ mouse: an excellent recipient mouse model for engraftment of human cells. Blood 2002;100:3175–3182.

17. Shultz LD, Lyons BL, Burzenski LM, et al. Human lymphoid and myeloid cell development in NOD/LtSz-scid IL2Rγnull mice engrafted with mobilized human hemopoietic stem cells. J Immunol 2005; 174:6477–6489.

18. Dolivo DM, Larson SA, Dominko T. Fibroblast growth factor 2 as an antifibrotic: antagonism of myofibroblast differentiation and suppression of pro-fibrotic gene expression. Cytokine Growth Factor Rev 2017;38:49–58.

19. Eto H, Suga H, Aoi N, et al. Therapeutic potential of fibroblast growth factor-2 for hypertrophic scars: upregulation of MMP-1 and HGF expression. Lab Invest 2012;92:214–223.

20. Kennedy SH, Rouda S, Qin H, Aho S, Selber J, Tan EM. Basic FGF regulates interstitial collagenase gene expression in human smooth muscle cells. J Cell Biochem 1997;65:32–41.

21. Lorenz HP, Longaker MT, Perkocha LA, Jennings RW, Harrison MR, Adzick NS. Scarless wound repair: a human fetal skin model. Development 1992;114:253–259.

22. Spyrou GE, Naylor IL. The effect of basic fibroblast growth factor on scarring. Br J Plast Surg 2002; 55:275–282.

23. Chinta M, Mascharak S, Borrelli MR, et al. Machine learning analysis of connective tissue networks enables objective characterization of skin fibroses. Plast Reconstr Surg Glob Open 2019; 7(4S):27–28.

24. Rinkevich Y, Walmsley GG, Hu MS, et al. Identification and isolation of a dermal lineage with intrinsic fibrogenic potential. Science 2015;348: aaa2151.

25. Driskell RR, Lichtenberger BM, Hoste E, et al. Distinct fibroblast lineages determine dermal architecture in skin development and repair. Nature 2013;504:277–281.

26. Philippeos C, Telerman SB, Oules B, et al. Spatial and single-cell transcriptional profiling identifies functionally distinct human dermal fibroblast subpopulations. J Invest Dermatol 2018;138:811–825.

27. Bikfalvi A, Klein S, Pintucci G, Rifkin DB. Biological roles of fibroblast growth factor-2. Endocr Rev 1997;18:26–45.

28. Nunes QM, Li Y, Sun C, Kinnunen TK, Fernig DG. Fibroblast growth factors as tissue repair and regeneration therapeutics. PeerJ 2016;4:e1535.

29. Akita S, Akino K, Hirano A. Basic fibroblast growth factor in scarless wound healing. Adv Wound Care (New Rochelle) 2013;2:44–49.

30. Park JW, Hwang SR, Yoon IS. Advanced growth factor delivery systems in wound management and skin regeneration. Molecules 2017;22:1259.

31. McGee GS, Davidson JM, Buckley A, et al. Recombinant basic fibroblast growth factor accelerates wound healing. J Surg Res 1988;45:145–153.

32. Borrelli MR, Irizzary D, Patel RA, et al. Pro-fibrotic CD26-positive fibroblasts are present in greater abundance in breast capsule tissue of irradiated breasts. Aesthet Surg J 2020;40:369–379.

33. Berking C, Takemoto R, Binder RL, et al. Photocarcinogenesis in human adult skin grafts. Carcinogenesis 2002;23:181–187.

34. Garcia M, Escamez MJ, Carretero M, et al. Modeling normal and pathological processes through skin tissue engineering. Mol Carcinog 2007;46:741–745.

35. Petratos PB, Chen J, Soslow RA, Bleustein CB, Felsen D, Poppas DP. Full-thickness human foreskin transplantation onto nude rats as an in vivo model of acute human wound healing. Plast Reconstr Surg 2003;111:1988–1997.

36. Walsh NC, Kenney LL, Jangalwe S, et al. Humanized mouse models of clinical disease. Annu Rev Pathol 2017;12:187–215.

37. Shultz LD, Brehm MA, Garcia-Martinez JV, Greiner DL. Humanized mice for immune system investigation: progress, promise and challenges. Nat Rev Immunol 2012;12:786.

38. Ito R, Takahashi T, Katano I, Ito M. Current advances in humanized mouse models. Cell Mol Immunol 2012;9:208.

Abbreviations and Acronyms

2D = two-dimensional
AF = Alexa Flour
FACS = fluorescence-activated cell sorting
FGF2 = fibroblast growth factor 2
H&E = hematoxylin and eosin
IL2rg = interleukin-2 receptor gamma chain
NSG = NOD scid gamma
P5–7 = postnatal days 5–7
PBS = phosphate buffered saline
PWD = postwound day
TSNE = t-Distributed Stochastic Neighbor Embedding